Nonisothermal Melt-Crystallization Kinetics of Isotactic Polypropylene Synthesized with a Metallocene Catalyst and Compounded with Different Quantities of an α Nucleator

T. Dobreva, J. M. López-Majada, J. M. Pereña, E. Pérez, R. Benavente

Instituto de Ciencia y Tecnología de Polímeros, Consejo Superior de Investigaciones Científicas (CSIC), Juan de la Cierva 3, 28006 Madrid, Spain

Received 11 October 2007; accepted 18 January 2008
DOI 10.1002/app.28105
Published online 17 April 2008 in Wiley InterScience (www.interscience.wiley.com).

ABSTRACT: The nonisothermal crystallization kinetics of a metallocene-made isotactic polypropylene (m-iPP) and its compounds with 0.1 wt % and 0.3 wt % of a sorbitol derivative [1,3:2,4-bis(3,4-dimethylbenzylidene)sorbitol (DMDBS); an α nucleator] were investigated by differential scanning calorimetry at different cooling rates from the melt. The nucleation efficiency was proved by a significant increase in the crystallization temperatures (accompanied by a slight augmentation of the degree of crystallinity and a decrease in the crystal sizes). This increase in the crystallization temperatures led to higher amounts of fractional content in the γ polymorph, even though DMDBS was supposed to be a nucleator for the α form. The Avrami and Ozawa methods effectively described only the early stage of crystallization, whereas a combined Avrami–Ozawa method was valid for the whole crystallization process. The values of the exponent for this method decreased for nucleated samples in the later stage of crystallization, especially in the case of m-iPP with 0.3 wt % DMDBS added (m-iPP03). The activation energy of the process and the surface free energy were also estimated. The production of considerable proportions of the γ polymorph in m-iPP03 corresponded to higher values of the activation energy and lower values of the surface free energy. © 2008 Wiley Periodicals, Inc. J Appl Polym Sci 109: 1338–1349, 2008

Key words: activation energy; crystallization; isotactic; nucleation; poly(propylene) (PP)

INTRODUCTION

The study of the nucleation of the crystallization process to improve the properties of isotactic polypropylene (iPP) has been done for many years as a response to the increased industrial use of iPP. Sorbitol-based derivatives, such as 1,3:2,4-bis(3,4-dimethylbenzylidene)sorbitol (DMDBS), are some commonly used nucleators for the α polymorph of iPP.[1–4] They have the advantage of dispersing in the molten polymer and recrystallizing on cooling into thin filaments, which yields a three-dimensional network.[1,2] In general, the nucleating efficiency is measured by an increase in the crystallinity, a decrease in the crystallization time, and the improvement of the optical transparency.[1–3] Maximum increases in the crystallization temperature and in the optical properties (transparency) of iPP due to the nucleation activity of DMDBS have been observed in compositions containing between 0.01 and 1 wt % of this nucleator.[2,4] A comparative study published for metallocene-made isotactic polypropylene (m-iPP) and conventional Ziegler–Natta isotactic polypropylene (ZN-iPP) polymers with 0.2% DMDBS at isothermal crystallization conditions showed that the nucleator is more effective with ZN-iPP than with m-iPP.[3]

Conventional ZN-iPP is capable of crystallizing into the following polymorphs: α (monoclinic), β (trigonal), γ (orthorhombic), and a mesomorphic crystal structure.[5–8] The most common and stable crystal structure is the α phase. The β phase is normally observed in the presence of nucleating agents[8–10] or under specific conditions such as a strong imposed orientation.[11] The γ phase has been obtained in conventional iPPs only under special conditions: elevated pressure, low molecular weight, and different ethylene contents in iPP/polyethylene random copolymers.[12,13] Finally, the mesomorphic phase dominates for samples efficiently quenched from the melt.[6,7,14]

Correspondence to: T. Dobreva (tdobreva@ictp.csic.es).

Contract grant sponsor: Ministerio de Educación y Ciencia; contract grant number: MAT 2005-00228.
Contract grant sponsor: Secretaría de Estado de Universidades e Investigación del Ministerio de Educación y Ciencia; contract grant number: SB2005-0016 (postdoctoral grant awarded to T.D.).
Contract grant sponsor: European Community Research Infrastructure Action; contract grant number: RII3-CT-2004-506008 (in support of the synchrotron work under the 6th Framework Program Structuring the European Research Area through the Integrated Infrastructure Initiative Integrating Activity on Synchrotron and Free Electron Laser Science).

On the contrary, m-iPPs usually crystallize from the melt in a disordered modification intermediate between the α (monoclinic) and γ (orthorhombic) forms, even at atmospheric pressure, and the amount of γ form present in the crystals depends on the crystallization conditions, molecular weight, concentration of defects, and ethylene content of the copolymers.[15–22] Fast cooling rates (V_0's) favor the appearance of the α polymorph, whereas the γ polymorph is favored at slow V_0's.[10,15,19] Moreover, both types of macromolecular defects, stereo and regio, lead to increases in γ phase. However, the crystallizable sequences increase with the crystallization temperature and pass through a maximum because their lengths depend on the temperature.[15,16] Therefore, at a given temperature, the γ polymorph begins decreasing.[15,21,22]

Kinetic studies provide a better understanding of the mechanism for the α + γ formation. The α and γ crystals grow together from the beginning of the crystallization, but the γ crystals melt first,[15,16] and the growth rate of the pure γ phase is lower than that of the α phase at isothermal conditions.[21] Moreover, the mother α lamellae appear first, and after that, the γ lamellae can grow.[12,21] Thus, the formation of crystals of the γ form needs more time than that of the α form.[22]

The main objective of this study was to analyze the melt-crystallization nonisothermal kinetics of pure m-iPP without nucleating agent (m-iPP00) and some samples with 0.1 and 0.3 wt % of a sorbitol derivative (DMDBS) added as a nucleator (m-iPP01 and m-iPP03, respectively). An attempt to observe the effect of the nucleation agent on the resulting microstructure was also performed by polarizing optical microscopy (POM) and atomic force microscopy (AFM).

EXPERIMENTAL

An m-iPP was used. It was obtained by a single-site homogeneous metallocene catalyst system and had the following characteristics: isotactic content = 87.8% mmmm pentads, regio defects r2.1 = 0.70; melt flow index (230°C, 2.16 kg) = 13.5 cm^3 (10/min); number-average molecular weight = 109 400 g/mol, and molecular weight distribution (weight-average molecular weight/number-average molecular weight) = 2.01. Irganox 1076 (0.2 wt %) (Ciba Co., Basel, Switzerland) was added as an antioxidant to reduce the thermal degradation.

The m-iPP and the nucleating agent DMDBS (Millad 3988) (Milliken and Co., Spartanburg, SC) were mixed in a Haake apparatus (Karlsruhe, Germany) at 180°C and 40 rpm for 10 min. Two different concentrations of DMDBS were added: 0.1 and 0.3 wt %, and the resulting compounds were named m-iPP01 and m-iPP03, respectively. All studies were compared with a sample of m-iPP00. The effect of the quantity of nucleating agent and the influence of different V_0's on the crystallization behavior were studied by differential scanning calorimetry (DSC) with a TA Instruments (New Castle, DE) Q100 calorimeter under a N_2 atmosphere. The samples were held 5 min at 200°C to remove the thermal history. Then, they were cooled at 11 different rates, ranging from 1 to 40°C/min, to a final temperature of 70°C. Afterward, each sample was heated at a rate of 10°C/min to 180°C.

The DSC results were complemented by POM with an Amplival Pol microscope from Carl Zeiss Jena (Oberkochen, Germany). The samples were prepared with melt crystallization techniques: thin films (100–190 μm) were sandwiched between a glass slide and a cover slip, with the sandwich slowly heated on a hot stage until the sample melted. With a thermal glove, a gentle pressure was applied to the cover slip to spread the liquid film, and the sample was then allowed to cool in air. The obtained crystals were analyzed after the sample was kept on the hot stage at 200°C for 5 min and were cooled subsequently at different rates, from 40 to 1°C/min.

The same polymeric films, washed with distilled water, were used for AFM multimode experiments, with a Nanoscope IVa scanning probe microscope (Veeco, Plainview, NY) at ambient conditions in the height mode.

The samples were also analyzed by wide-angle X-ray scattering with synchrotron radiation. These studies were performed in the soft-condensed matter beamline A2 at Hamburger Synchrotronstrahlungslabor (Hamburg, Germany), at a wavelength of 0.150 nm. A charge coupling device detector MARCCD 165 from Rayonix LLC (Evanston, IL) was used, located at a distance of 17 cm from the sample (which was inside the temperature controller of the beamline). A sample of silver behenate (which gave a well-defined diffraction at a spacing of 5.838 nm and several orders) was used for calibration. The samples were cooled from the melt (180°C) at a rate of 8°C/min, with images acquired every 15 s. The two-dimensional X-ray patterns were processed with the FIT2D program of Dr. Hammersley (the European Synchrotron Radiation Facility, ESRF, Grenoble, France) and converted into one-dimensional arrays after normalization for the intensity of the primary beam and subtraction of the scattering of an empty sample.

RESULTS AND DISCUSSION

Nonisothermal crystallization kinetics

The DSC scans showed typical crystallization peaks for the three samples of m-iPP at various V_0's (Fig. 1). The enthalpy of crystallization (ΔH_c), the onset temperature (T_0), and the peak crystallization temperature (T_c) were determined from the nonisothermal exotherms and are listed in Table I. The degree

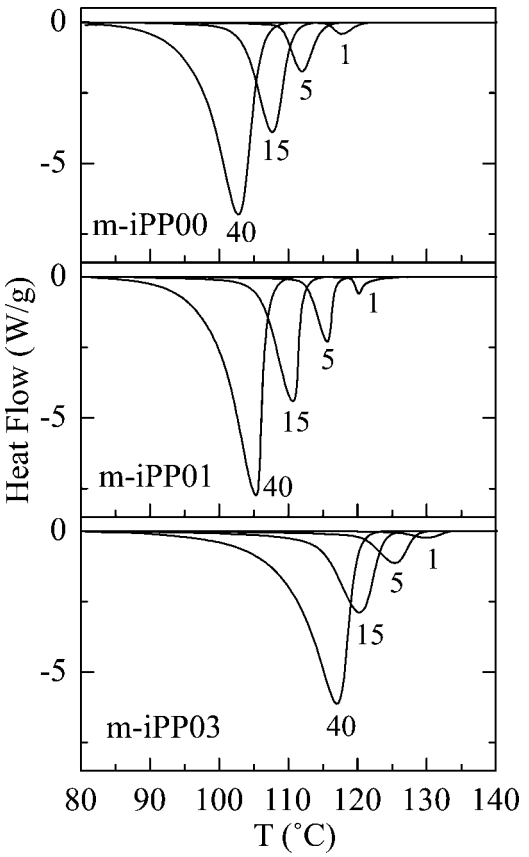

Figure 1 DSC cooling curves for the three m-iPP samples at the indicated selected V_0's.

of crystallinity (X_c), also shown in Table I, was calculated from ΔH_c with the following relation:

$$X_c = \Delta H_c / \Delta H_m^o \quad (1)$$

where ΔH_m^o is the heat of fusion for 100% crystalline folded chains of iPP, with a value of 209 J/g [23] corresponding to the α polymorph. The value for the γ form was expected to be rather similar.[10]

The results in Table I clearly indicate that the addition of DMDBS led to a slight increase in X_c and a significant augmentation of the crystallization temperature at the various nucleator concentrations. This effect is clearly shown in Figure 2, where an increase in the crystallization temperature of around 2–3°C was obtained for specimen m-iPP01 in relation to the pure polymer, whereas that increase was as high as 13°C for sample m-iPP03. Therefore, the nucleating agent shifted the process of crystallization toward higher temperatures because of the nucleation activity. On the other hand, the slower V_0's related to the higher X_c for the three investigated polymer samples. These results were in agreement with published data for ZN-iPP, where the X_c changed slightly for DMDBS contents between 0.01 and 1 wt %.[2]

Normally, the crystallization peaks are single for m-iPP because the two types of crystals (α+γ) are formed simultaneously,[21] although the growth of γ crystals is initially influenced by α crystals.[12] On the contrary, the melting process is characterized by dual peaks: one for the melting of the γ polymorph and the other corresponding to the α crystals (see Fig. 3). The two melting peaks prove the polymorphism of m-iPP, and it was clear that the two polymorphs coexisted for all V_0's.

The deconvolution of these dual melting peaks allows one to estimate the fractional content of the two modifications. Because the corresponding enthalpies of melting are reported to be rather similar,[10,13] those fractional contents were taken just as the relative enthalpies below each endotherm component. The corresponding results are shown in the left frame of Figure 4 as a function of V_0 for the three m-iPP samples. It was very evident that the fraction of γ modification over the total crystals increased as V_0 decreased, as expected, and that the γ content for a given V_0 increased with the amount of nucleating agent.

Interestingly, when the fraction of γ modification was plotted against T_c, as presented in the right frame of Figure 4, a common line was obtained for the three samples. The conclusion from this behavior was that the DMDBS nucleator did not have a specific influence on the nucleation of a particular modification. However, its nucleation ability, that is, the increase in the crystallization rate, and, therefore, the achievement of the crystallization at higher temperatures led to higher amounts of the γ phase.

On the other hand, and as was discussed previously, the fraction of γ modification was reported to pass through a maximum at relatively high crystallization temperatures.[15] In this case, such a maximum was not observed because it appears in the region of rather slow crystallization rates, typical of isothermal experiments. However, and considering the defect content of this m-iPP sample (see the Experimental section), that maximum may be[15] around 130°C, which was the upper limit of our experiments.

Another quantification of the relative amount of the two polymorphs could be obtained from diffraction data. We performed some diffraction experiments on the three samples by cooling from the melt at 8°C/min in a synchrotron source. The final diffractograms (at room temperature) of these experiments are shown in Figure 5. The diffractograms for the α and γ modifications[6,7,10,15] were rather similar except for the well-distinguished diffractions at a scattering vector (s)-1/d = 2.09 mm^{-1} for the α modification ([130] reflection) and at 2.26 mm^{-1} for the γ form ([117] reflection). It was evident from the inspection of these diffractions in Figure 5 that at this V_0 of 8°C/min, the majority of the crystals were of the α type for specimens m-iPP00 and m-iPP01,

TABLE I
Values of ΔH_c, T_0, T_c, X_c, and $t_{1/2}$ for m-iPP00, m-iPP01, and m-iPP03 at Various V_0 Values

Specimen	V_0 (°C/min)	ΔH_c (J/g)	T_0 (°C)	T_c (°C)	X_c	$t_{1/2}$ (min)
m-iPP00	1	87.1	123.0	117.7	0.417	5.24
	2	87.9	120.4	115.4	0.421	2.53
	3	87.3	119.2	113.8	0.417	1.8
	5	85.6	117.4	111.9	0.409	1.12
	7	83.3	116.3	110.7	0.399	0.83
	10	82.3	114.9	109.3	0.394	0.61
	12	79.9	114.2	108.7	0.383	0.51
	15	78.4	113.3	107.6	0.375	0.43
	20	77.9	112.1	106.4	0.373	0.33
	30	74.6	110.3	104.3	0.357	0.23
	40	73.9	109.0	102.7	0.354	0.19
m-iPP01	1	91.4	127.8	120.2	0.437	7.4
	2	89.9	123.2	118.6	0.430	2.5
	3	88.8	121.2	117.3	0.425	1.5
	5	85.9	119.2	115.6	0.411	0.9
	7	84.0	117.7	114.3	0.402	0.6
	10	82.2	116.3	112.8	0.393	0.5
	12	80.9	115.5	111.8	0.387	0.4
	15	79.1	114.5	110.7	0.378	0.33
	20	76.9	113.2	109.2	0.368	0.28
	30	73.6	111.2	107.1	0.352	0.2
	40	71.6	109.8	105.4	0.343	0.16
m-iPP03	1	95.1	134.8	129.9	0.455	6.2
	2	93.6	133.0	128.2	0.448	3
	3	91.9	131.4	126.2	0.440	2.1
	5	90.9	130.3	125.4	0.435	1.3
	7	88.4	128.8	123.2	0.423	0.98
	10	86.2	128.3	122.9	0.413	0.68
	12	85.6	127.1	121.1	0.41	0.6
	15	83.9	126.3	120.3	0.401	0.5
	20	82.9	125.4	120.2	0.397	0.35
	30	80.2	123.6	117.6	0.384	0.28
	40	77.9	122.6	117.0	0.373	0.2

whereas rather similar proportions of α and γ modifications coexisted in specimen m-iPP03. In fact, the corresponding deconvolution of the diffractograms shown in Figure 4 led to the following fractions of γ modification: 0.25, 0.30, and 0.50% for m-iPP00, m-iPP01, and m-iPP03, respectively. These values, represented as full points in the left frame of Figure 4, were rather similar to those obtained from the DSC melting curves.

On the other hand, we applied several kinetic models to study the behavior during the nonisothermal conditions. Figure 6 presents the relative degree of crystallinity (X_t) as a function of crystallization temperature (T) with the following expression:

$$X_t = \int_{T_0}^{T} (dH_c/dT)dT \Big/ \int_{T}^{T_\infty} (dH_c/dT) \qquad (2)$$

where T_0 and T_∞ are the onset and end temperatures of crystallization, and H_c is the enthalpy of crystallization, respectively.

Afterward, the temperature parameter was converted into a timescale by

$$t = (T_0 - T)/V_0 \qquad (3)$$

where T is the temperature at crystallization time t. Typical plots of X_t as a function of time are illustrated in Figure 7. An important parameter that can be obtained directly from this plot is the half time of crystallization ($t_{1/2}$), which corresponds to the 50% completion of crystallization. The corresponding values are also listed in Table I. It was apparent that the crystallizations of m-iPP01, once started, were completed faster than the ones for m-iPP03. However, according to the values of T_c, the nucleation activity was rather important in m-iPP03. We expect, as found experimentally, that the shifting of the crystallization process to higher temperatures favored the growth of the γ polymorph and that the γ crystals needed more time to grow.[18,21]

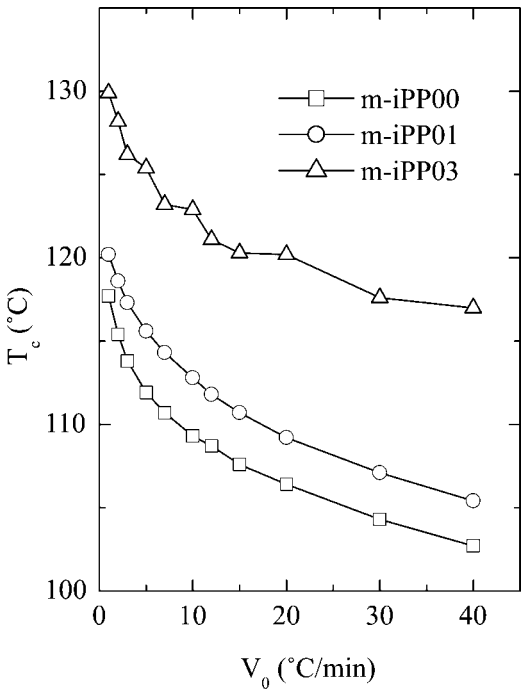

Figure 2 Variation of T_c with V_0 for the three m-iPP samples.

The melt crystallization of polymers is usually a nucleation-controlled process that involves the following important steps: the diffusion of crystallizable chains to the crystal front, the formation of a stable nucleus, and crystal growth. The determination of the kinetic parameters, such as the activation energy and the surface free energy, enabled us to obtain a better understanding of how the nucleating agent DMDBS affected the crystallization behavior of m-iPP, as is discussed later.

Moreover, information about the crystal growth rate and nucleation mode could be deduced from the application of the nonisothermal crystallization conditions of the well-known Avrami equation:

$$X_t = 1 - \exp(-kt^n) \tag{4}$$

where k is a rate constant for the crystallization process and is proportional to the concentration of

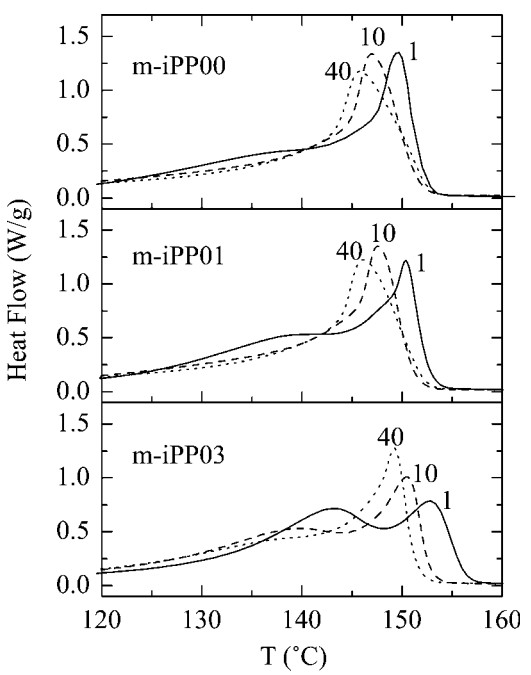

Figure 3 DSC melting endotherms recorded at 10°C/min for the three m-iPP samples after they were cooled from the melt at the indicated V_0's.

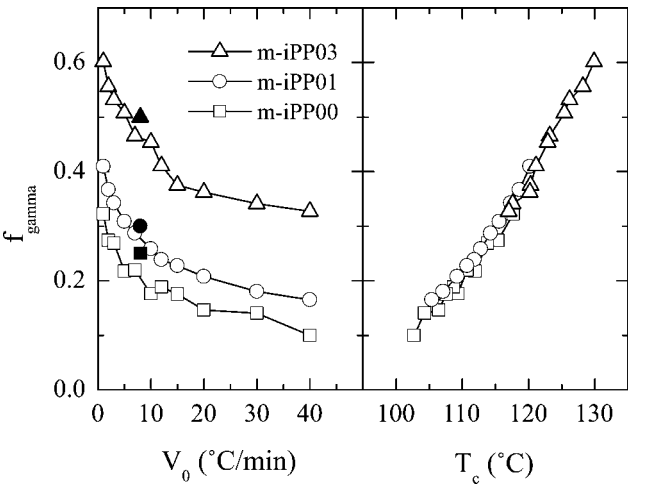

Figure 4 Variation of the fractional content of γ modification (deduced from the melting curves) with (left) V_0 and (right) T_c for the three m-iPP samples. The full points in the left frame represent the values obtained from the diffractograms in Figure 5.

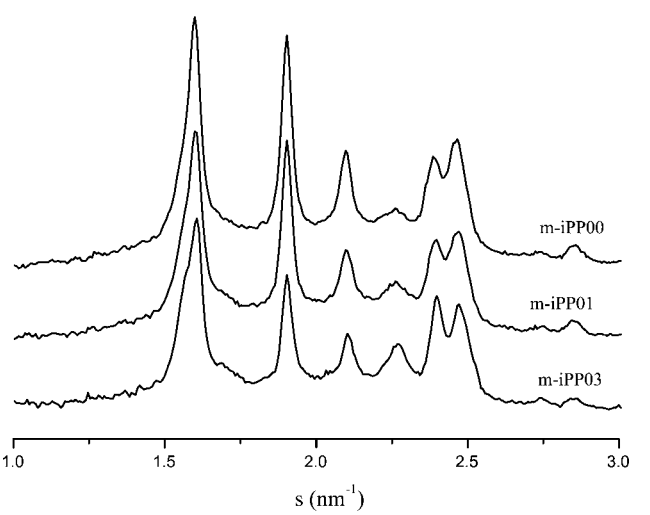

Figure 5 X-ray diffractograms acquired at room temperature for the three m-iPP samples cooled from the melt at 8°C/min.

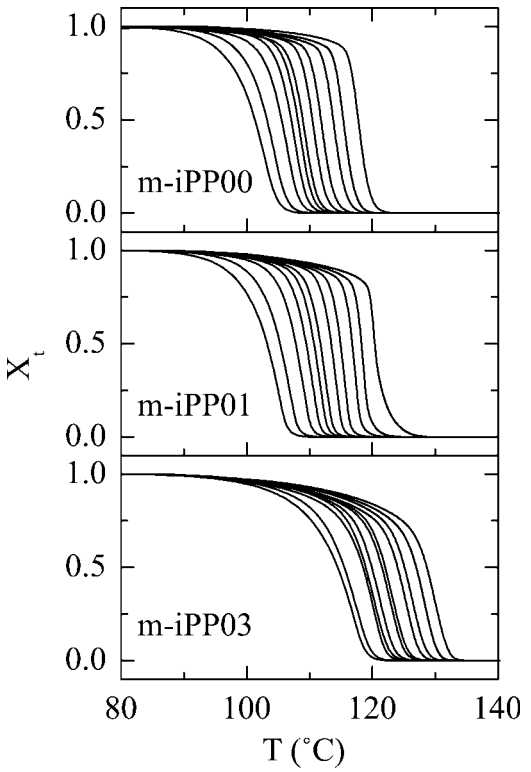

Figure 6 X_t versus temperature for the three investigated samples at different V_0's. From right to left: 1, 2, 3, 5, 7, 10, 12, 15, 20, 30, and 40°C/min.

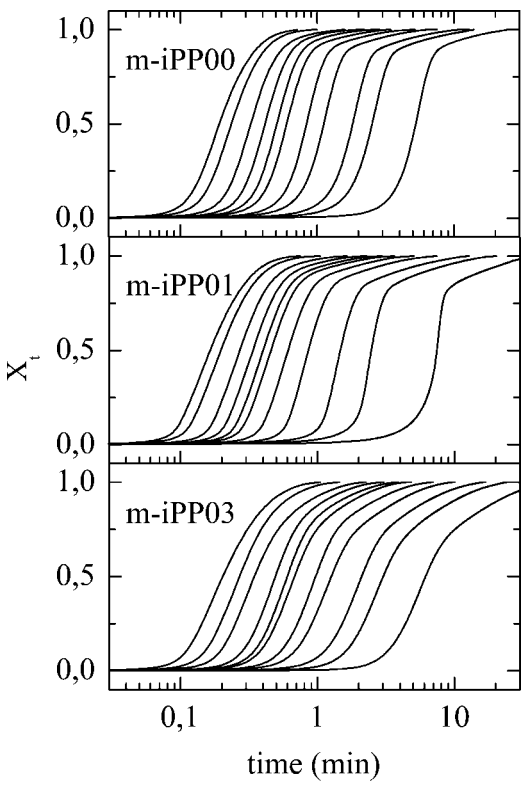

Figure 7 X_t versus time for the three m-iPP samples at different V_0's. From right to left: 1, 2, 3, 5, 7, 10, 12, 15, 20, 30, and 40°C/min.

nuclei. The Avrami exponent (n) depends on the morphology of the growing crystalline regions and the nucleation process. This empirical equation, initially formulated for isothermal experiments, has been also successfully used to describe the nonisothermal crystallization of polymers.[24–27] In such cases, the parameters n and k do not have the same physical meaning as in isothermal conditions because the temperature changes constantly during nonisothermal crystallization. The double logarithm of the Avrami equation gives the following relationship:

$$\ln[-\ln(1 - X_t)] = \ln k + n \ln t \quad (5)$$

Consequently, a plot of $\ln[-\ln(1 - X_t)]$ versus $\ln t$ would yield a straight line if the equation is fulfilled. The corresponding plots, from the data in Figure 7, are presented in Figure 8. Fairly good straight lines were obtained up to crystallization conversions of around 0.7, followed by a significant deviation during the later stage of crystallization. This deviation is usually considered to be due to the presence of secondary crystallization, which causes a slow down of crystallization and further perfection of crystals in the later stage.

The kinetic data in the early stage were used to estimate the Avrami parameters for the nonisothermal crystallization of the m-iPPs. The values of n

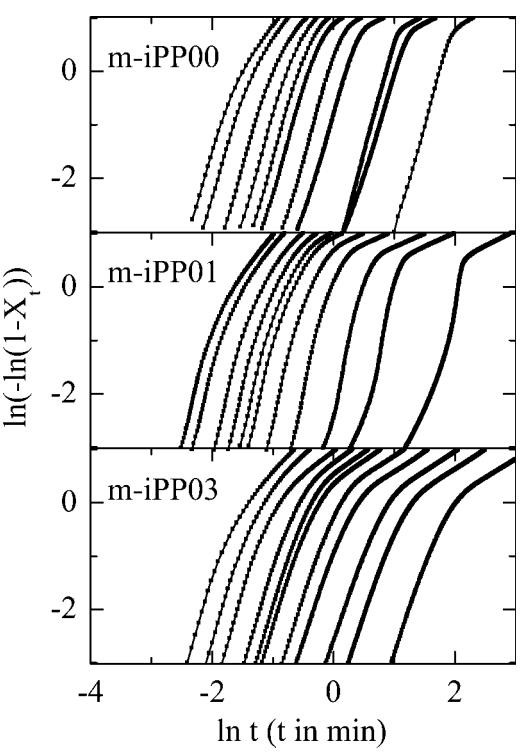

Figure 8 Avrami plots for the three m-iPP samples at different V_0's. From right to left: 1, 2, 3, 5, 7, 10, 12, 15, 20, 30, and 40°C/min.

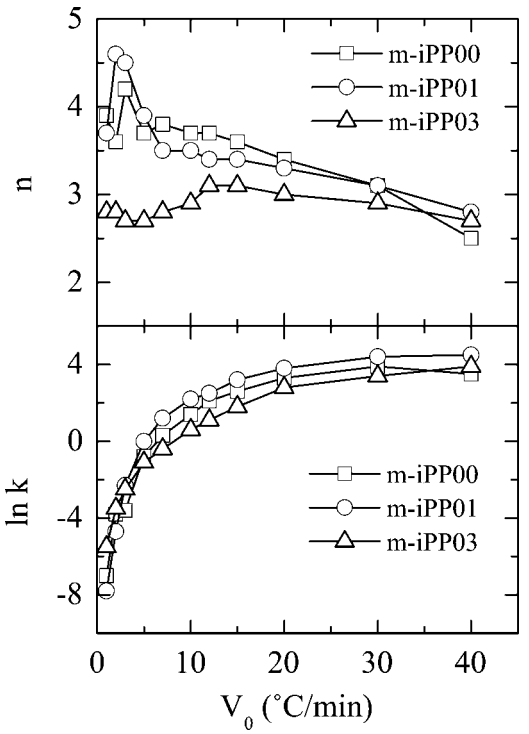

Figure 9 Results for n and for the kinetic parameter ln k for the three m-iPP samples as a function of V_0.

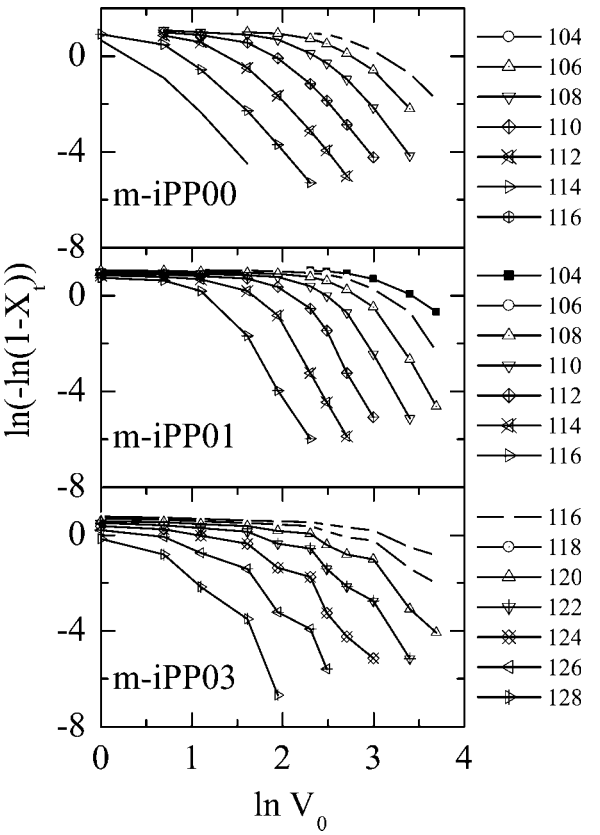

Figure 10 Ozawa plots for the three m-iPP samples at the indicated temperatures.

and the rate parameter ln k, determined from the slopes and intercepts of the initial straight lines, are shown in Figure 9. The lowest values of n were obtained for specimen m-iPP03, especially for the lower V_0's. The average values of n were 3.6, 3.6, and 2.8 for m-iPP00, m-iPP01 and m-iPP03, respectively. The noninteger values of n could have been due to crystal branching, two-stage crystal growth, or mixed growth.[28] These values of n seemed to indicate three-dimensional spherulitic growth for m-iPP00 and m-iPP01 and two-dimensional growth of lamellar crystals for m-iPP03. On the other hand, the crystallization rates (ln k) and also the number of nuclei increased with increasing V_0 for the three samples.

The Avrami equation was found invalid in the later stages, for secondary crystallization, when the spherulites had generally impinged and a deviation from linearity appeared. Ozawa[29] modified the Avrami equation by incorporating the V_0 factor, as follows:

$$X_T = 1 - \exp\left[-K(T)\right]/V_0^m \tag{6}$$

where X_T is the relative crystallinity at temperature T, $K(T)$ is the cooling rate function, and m is the Ozawa exponent. The double logarithm of the Ozawa equation gives the following relationship:

$$\ln[-\ln(1 - X_T)] = \ln[K(T)] - m \ln V_0 \tag{7}$$

If the Ozawa method could have correctly described the nonisothermal crystallization process of m-iPP, the corresponding plots would have given a series of parallel lines with slope m and intercept $K(T)$. However, Figure 10 shows again that straight lines were only observed in the early stages of crystallization. Therefore, m and $K(T)$ were estimated from the initial straight sections in the early crystallization stages for the three iPP samples. The results are shown in Table II. A great scattering in the slope was

TABLE II
Results for m and the Kinetic Rate Parameter ln k for the Nonisothermal Crystallizations of the Three Investigated Polymer Samples

	m-iPP00		m-iPP01		m-iPP03	
Temperature (°C)	m	ln k	m	ln k	m	ln k
108	3.4	7.7	4.4	12.0		
110	3.5	6.5	5.0	12.7		
112	3.5	4.8	5.3	11.3		
114	3.6	3.2	5.7	9.8		
116	3.9	1.8	5.2	6.2		
120					2.9	7.2
122					3.9	8.6
124					3.5	5.6
126					3.4	3.4
128					4.3	2.5

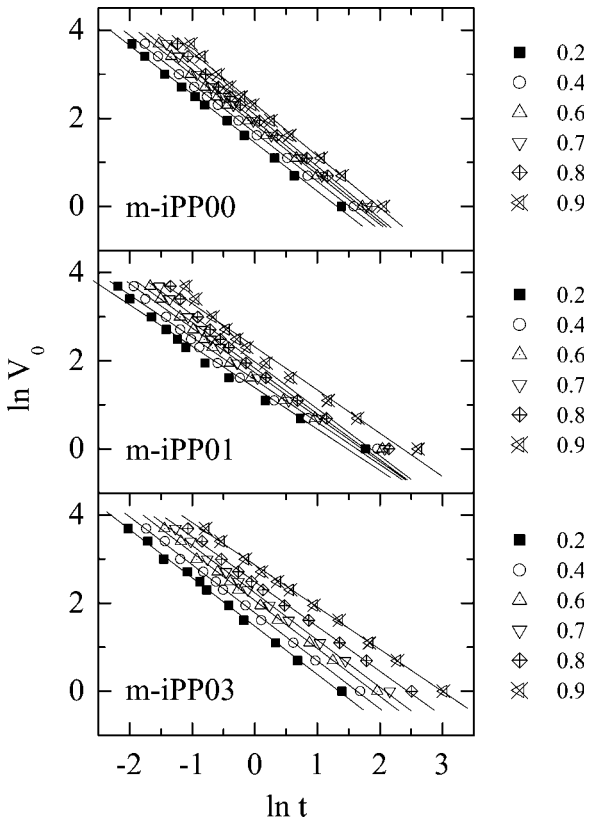

Figure 11 Plots of ln V_0 versus ln t for the three m-iPP samples at the indicated X_t's.

observed, although, again, the values of the exponent were the lowest for sample m-iPP03, and it was very evident that the crystallization shifted to a higher temperature.

In conclusion, the Ozawa analysis could not adequately describe the nonisothermal crystallization kinetics of m-iPPs.

Using a different kinetic equation proposed by Liu et al.,[30] which combines the Avrami and Ozawa equations, we obtained a good crystallization description of these m-iPPs. As the Avrami equation relates X_t with time t and the Ozawa equation relates X_t with V_0, a relation between V_0 and t could be established to connect these two equations. Thus, for a given X_c, it follows from eqs. (5) and (7) that

$$\ln k + n \ln t = \ln[K(T)] - m \ln V_0 \tag{8}$$

This equation could be rearranged as follows:

$$\ln V_0 = \ln[F(T)] - a \ln t \tag{9}$$

where $F(T) = [K(T)/k]^{1/m}$ is the kinetic parameter of the measured system and $a = n/m$ is the ratio between the Avrami and Ozawa exponents.

It is apparent from Figure 11 that the method developed by Liu et al.[30] was successful in describing the nonisothermal crystallization behavior of the original and the nucleated m-iPP samples. The parameters obtained from these straight lines are listed in Table III. The $F(T)$ values increased with increasing X_t for the three different samples. Moreover, at the given X_t, the relative kinetic parameters [$F(T)$'s] of m-iPP03 were higher than those of m-iPP01 and m-iPP00.

On the other hand, the values of parameter a, which depend on the growth mode, were practically constant for the three samples up to a crystallinity of around 0.7 but differed in the later stage of crystallization. The exponent a for m-iPP00 increased, whereas that for m-iPP03 decreased, in the later stage of crystallization, that is, when γ lamellae grew, generally by a branching mechanism, over α lamellae.[12,17,21] Moreover, there was not a great difference in the nucleation and growth mechanisms of crystals during the initial stage of crystallization, when α lamellae predominantly grow.

A study of ZN-iPP with DMDBS showed that the nucleating agent can crystallize to form thin fibril-like structures.[1,2] Generally, much more γ polymorph was obtained for m-iPP than for ZN-iPP, and the addition of DMDBS caused two effects: a shift of the crystallization to higher temperatures and the formation of a network of thin fibrils, both of which the appearance of the γ polymorph.

This combined method has also been proved to be effective in a number of polymeric systems, such as polypropylene–polypropylene/grafted maleic anhydride–organic montmorillonite,[25] nylon 1313,[26] and poly(9,9-dihexylfluorene)-*alt*-*co*-(1,4-phenylene).[27]

Morphology observations

The observation of the crystal structures of m-iPPs by means of POM indicated that the perfection of the structures decreased with increasing V_0 for the three polymeric systems. Figure 12 presents the crystal morphology for the m-iPPs crystallized at 1°C/min and shows a typical disordered pattern between the α and γ lamellae.[17,18,21] Moreover, the nucleating

TABLE III
Nonisothermal Crystallization Kinetic Parameters at Different X_t's from the Avrami/Ozawa Combined Method

		X_t					
		0.2	0.4	0.6	0.7	0.8	0.9
m-iPP00	a	1.1	1.1	1.1	1.1	1.2	1.2
	$F(T)$	3.0	5.5	6.4	6.7	8.2	10.0
m-iPP01	a	0.9	1.0	1.0	1.0	1.0	0.9
	$F(T)$	3.0	5.0	5.5	6.0	6.0	9.0
m-iPP03	a	1.1	1.1	1.1	1.1	1.0	0.95
	$F(T)$	4.5	6.0	8.2	9.0	12.2	18.2

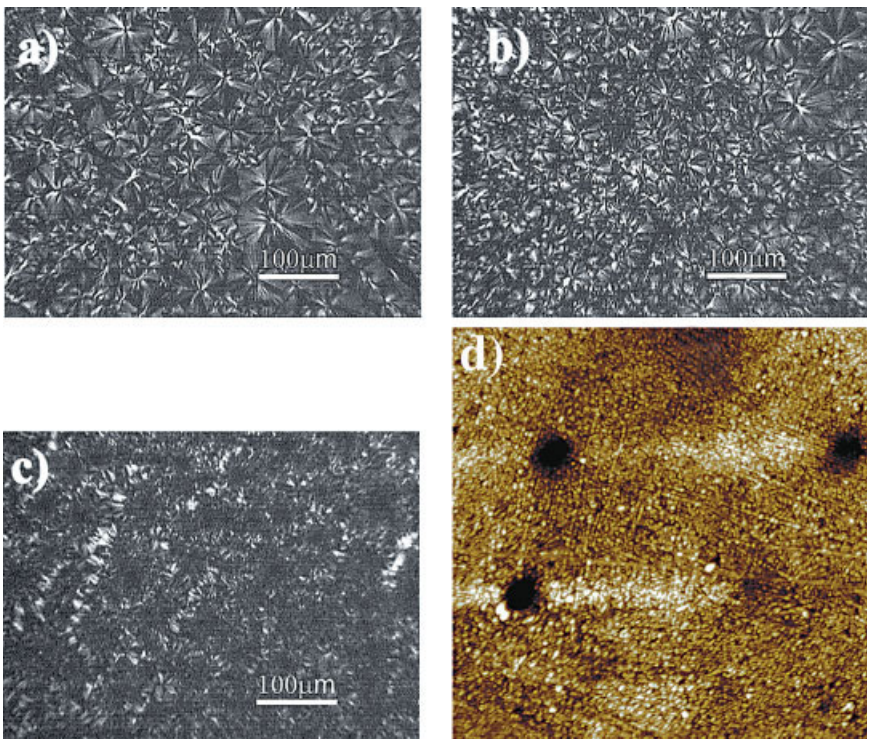

Figure 12 Optical micrographs of (a) m-iPP00, (b) m-iPP01, and (c) m-iPP03 and (d) a topographic AFM image (2.5 × 2.5 μm^2) of m-iPP03. All of the samples were crystallized nonisothermally at a V_0 of 1°C/min. [Color figure can be viewed in the online issue, which is available at www.interscience.wiley.com.]

additive led to a significant decrease in the crystal sizes.

The observation of the morphology with a quarter-wave plate (1/4λ plate) located diagonally between crossed polars showed positive spherulitic structures for m-iPP00 and m-iPP01 at lower V_0's and ones with mixed birefringence for V_0's higher than 10°C/min. For m-iPP03, however, only several lamellae, which presumably were part of a spherulitic skeleton, were exhibited. Only yellow or blue areas could be observed, and it was impossible to measure the birefringence. The model of Alamo et al.[21] was proven by optical micrographs of m-iPP03, where the γ phase predominated [Fig. 12(c)]. A network of thin fibrils could be seen in AFM topographic microphotos of m-iPP03 [Fig. 12(d)].

Activation energy of crystallization

To evaluate the activation energy (ΔE) of crystallization for the transport of polymer chains toward the growing surface, the method of Kissinger[31] was applied. When one considers the variation of T_c with V_0, the activation energy can be determined by the following equation:

$$\log\left(\frac{V_0}{T_c^2}\right) = -\frac{\Delta E}{R}\frac{1}{T_c} \tag{10}$$

The results obtained from Figure 13 were 309 kJ/mol for m-iPP00 and 304 and 363 kJ/mol for m-iPP01 and m-iPP03, respectively. For comparison, ΔE for ZN-iPP calculated by the same method was 216 kJ/mol.[32] Because the crystallization activation energy is usually regarded as an indication of the crystallization ability of polymers, it follows that m-iPP01 possessed the highest crystallization ability

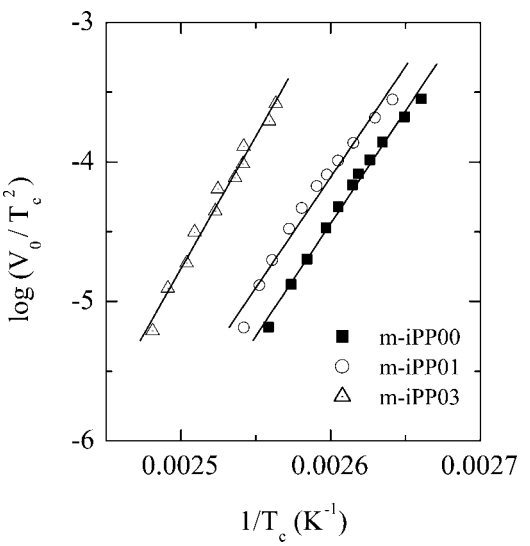

Figure 13 Kissinger plots for the three m-iPP samples.

and that a strong interaction between the nucleating agent and macromolecular chains interfered in the crystallization growth of m-iPP03. This result was in a good agreement with $t_{1/2h}$, which was again the highest. Moreover, because the crystallization temperature was augmented and the γ form predominated, shorter crystallizable sequences could have participated during the crystallization of m-iPP03. The molecular mobility of these γ crystallizable sequences was hindered, which was reflected in a higher value of the activation energy for this polymer system.

Surface free energy

The study of the surface free energy was carried out with eq. (11) for the total rate of the nonisothermal crystallization, according to refs. 33–35:

$$G_c = V_0\left[(dH/dT)T_n/\Delta H_m^o\right]\left[\int_0^\infty (dH/dT)dT\right] \Big/ \left[\int_{T_n}^\infty (dH/dT)dT\right] \quad (11)$$

where G_c is the total rate at the temperature T_n, dH/dT is the enthalpy for a given narrow temperature range at the current temperature T_n, $\int_0^\infty (dH/dT)dT$ is the crystallization enthalpy of the whole process, and $\int_{T_n}^\infty (dH/dT)dT$ is the enthalpy of the quantity of substance that remains to be transformed into the other phase and represents the correction function. The depletion of the crystallizing polymer is included in this correction function. Therefore, eq. (11) defines the whole crystallization process as a series of isothermal processes at the corresponding infinitesimal temperature intervals.

Mathematically, the nucleation-controlled growth of crystallites with chain folding can be simply expressed in terms of a biexponential equation according to the theory of Hoffman and coworkers:[36–39]

$$G_c = G_0 \exp[-U^*/R(T - T_{\inf})] \exp\left[-K_g/T\Delta Tf\right] \quad (12)$$

where G_c is the growth rate at a specific temperature T, G_0 is a preexponential factor, and the term in the first exponential is associated with segmental transport across the crystal/amorphous interface. Thus, U^* is the activation energy for polymer diffusion across the phase boundary, R is the gas constant, and $T_{\inf}$ is the temperature below which segmental motion becomes infinitely slow and is usually expressed as $T_{\inf} = T_g - 30$ K, where T_g is the glass-transition temperature. The second exponential in eq. (12) accounts for the free energy contribution for the growth of a critical size nucleus, which is inversely proportional to the undercooling, $\Delta T = T_m^o - T$, where T_m^o is the equilibrium melting temperature, and to the correction factor $f = 2T_c/(T_m^o + T)$ for variations in the heat of fusion. On the other hand, the free energy term also depends on the nucleation rate constant (K_g), which is expressed as

$$K_g = \frac{zb_0\sigma\sigma_e T_m^o}{\Delta H_m^o k} \quad (13)$$

where b_0 is the thickness of the growing layer, σ and σ_e are the lateral and fold surface free energies, ΔH_m^o is the heat of fusion, and k is the Boltzmann constant. The factor z depends on the growth regime, and it takes the value of 4 for regimes I and III and 2 for regime II.[37,38]

The rearrangement of eq. (12) leads to

$$\log G_c + \frac{U^*}{2.303R(T - T_{\inf})} = \log G_o - \left(\frac{K_g}{2.303T\Delta Tf}\right) \quad (14)$$

so that a plot of $\log G_c + U^*/2.303R(T - T_{\inf})$ versus $1/T\Delta Tf$ will allow one to obtain K_g from the corresponding straight line, if such an equation is fulfilled.

These analyses were applied to the crystallization rate data deduced from eq. (11). The corresponding plots for some selected V_0's are shown in Figure 14, where the following parameters were used: U^* = 6276 J/mol, T_g = 259 K, T_m^o = 459 K, and ΔH_m^o = 1.96×10^8 J/m^3.[3,37,38]

Fairly good straight lines were observed in the initial stages of the crystallization, with rather similar slopes for the different V_0's. The corresponding average values for K_g are presented in Table IV. Values of K_g between 3 and 6×10^5 K^2 were reported for the isothermal crystallization of conventional ZN-iPP[38] and around 3×10^5 K^2 for a metallocenic iPP.[3] The values in this case were, therefore, around three to four times higher, which should have been reflected in the correspondingly higher values for the product of the surface free energies, as deduced from eq. (13).

Taking into account that the crystallization temperatures here analyzed were in the range from around 70 to 134°C (as shown in Figs. 1 and 5), we considered that all of the experiments fell into regime III[37,39] so that the factor z in eq. (14) was 4. On the other hand and with an assumed value of b_0 = 0.626 nm for the growth of iPP in the (110) plane of the monoclinic α form of iPP [which was practically coincident with the value of 0.640 nm for the (111)

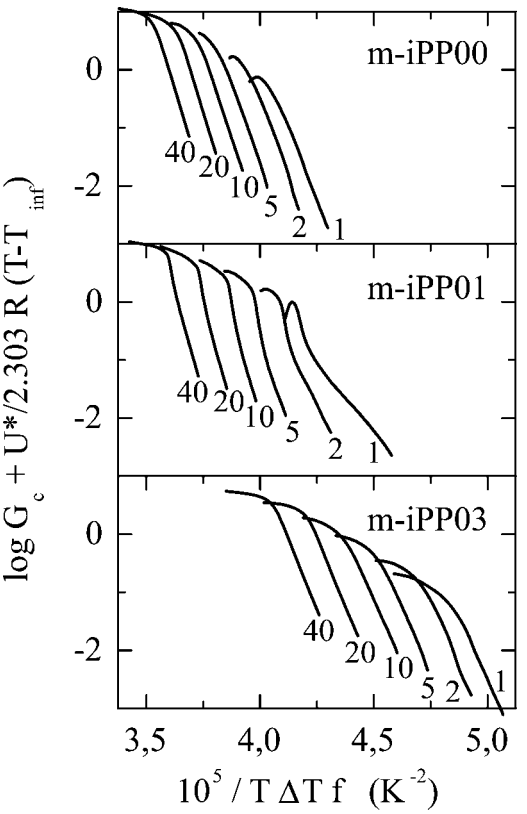

Figure 14 Plots of eq. (13) for the three investigated samples at the indicated selected V_0's.

plane of the orthorhombic γ modification], the product of the two surface free energies was determined, and the values are shown in Table IV.

σ is usually estimated from the enthalpy of melting,[37] and a value of 11.5 mJ/m^2 was deduced. With this information, σ_e was estimated, and the corresponding values are also shown in Table IV. These results were, again, considerably higher than those previously reported for the isothermal crystallization of iPP.[37,39] The discrepancy may have arisen from the fact that in this case of nonisothermal crystallization, the process was carried out at variable temperatures and the obtained crystals may have had, presumably, different surface free energies than those in the isothermal case. Moreover, the approximation for σ may not be applicable to nonisothermal crystallization. When these were the case, we could estimate the surface free energy on average from the product of σ and σ_e, just by applying the square root. In such case, the corresponding average values (σ_{ave}'s) are shown in the last columns of Table IV. Curiously, the values so obtained were rather similar to those reported for σ_e in isothermal crystallization,[37,39] which were around 65–70 mJ/m^2.

Independent of these approximations, it follows from the results in Table IV that the K_g and the product of the surface free energies presented the lowest values for specimen m-iPP03, which indicated, most probably, the existence of more chain folding irregularities due to the higher proportion of γ crystals in this sample.

CONCLUSIONS

As deduced from DSC and X-ray experiments, the addition of the nucleating agent DMDBS to m-iPP caused the formation of higher amounts of γ crystals in relation to the raw polymer, even though DMDBS is supposed to be a nucleator for the α form. The reason was that with the addition of the nucleator, the whole crystallization shifted toward higher temperatures, where the γ formation was favored. Thus, when the fraction of γ modification was plotted against T_c, a common line was obtained for the three samples analyzed. Our conclusion from this behavior was that the DMDBS nucleator did not have a specific influence on the nucleation of a particular modification. However, its nucleation ability, that is, the increase in the crystallization rate, and, therefore, the achievement of the crystallization process at higher temperatures led to higher amounts of the γ phase.

Avrami's theory was valid for the primary crystallization up to 70%. The determined n values indicated three-dimensional spherulitic growth and homogeneous nucleation for m-iPP00 and m-iPP01 and two-dimensional structures and heterogeneous nucleation for m-iPP03 due to the crystal branching growth mechanism.

Similarly, the Ozawa equation described only the early stage of crystallization.

A combined model between the Avrami and Ozawa equations was, however, valid for the whole crystallization process. The values of the exponent for this method decreased for nucleated samples in the later stage of crystallization, especially in the case of m-iPP03.

The activation energy of the process and the surface free energy were also estimated. The production of considerable proportions of the γ polymorph in m-iPP03 corresponded to higher values of the activation energy and lower values of the surface free energy.

TABLE IV
Values of K_g and the Surface Free Energies for the Three m-iPP Samples

Sample	10^5 K_g (K^2)	$\sigma\sigma_e$ (mJ^2/m^4)	σ_e (mJ/m^2)	σ_{ave} (mJ/m^2)
m-iPP00	11	5950	520	77
m-iPP01	12	6450	560	80
m-iPP03	8.7	4700	410	68

The authors are grateful to Milliken Co. for supplying the nucleating agent. They also thank the collaboration of Hamburger Synchrotronstrahlungslabor personnel in the soft-condensed matter beamline A2.

References

1. Fillon, B.; Lotz, B.; Thierry, A.; Wittmann, J. C. J Polym Sci Part B: Polym Phys 1993, 31, 1395.
2. Kristiansen, M.; Werner, M.; Tervoort, T.; Smith, P. Macromolecules 2003, 36, 5150.
3. Varma-Nair, M.; Agarwal, P. K. J Therm Anal Calorim 2000, 59, 483.
4. Romankiewicz, A.; Sterzynski, T.; Brostow, W. Polym Int 2004, 53, 2086.
5. Maier, G.; Calafut, T. Polypropylene. The Definitive User's Guide and Databook; Plastics Design Library: Norwich, NY, 1998; p 11.
6. Phillips, P. J.; Mezghani, K. In The Polymeric Materials Encyclopedia; Salamone, J. C., Ed.; CRC: Boca Raton, FL, 1996; Vol. 9, p 6637.
7. Brückner, S.; Meille, S. V.; Petraccone, V.; Pirozzi, B. Prog Polym Sci 1991, 16, 361.
8. Varga, J. In Polypropylene: Structure, Blends and Composites; Karger-Kocsis, J., Ed.; Chapman & Hall: London, 1995; Vol. 1, p 56.
9. Varga, J. J Mater Sci 1992, 27, 2557.
10. Krache, R.; Benavente, R.; López-Majada, J. M.; Pereña, J. M.; Cerrada, M. L.; Pérez, E. Macromolecules 2007, 40, 6871.
11. Davies, R. J.; Zafeiropoulos, N. E.; Schneider, K.; Roth, S. V.; Burghammer, M.; Riekel, K.; Kotek, J. C.; Stamm, M. Colloid Polym Sci 2004, 282, 854.
12. Lotz, B.; Graff, S.; Staupe, C.; Wittmann, J. C. Polymer 1991, 32, 2902.
13. (a) Mezghani, K.; Phillips, P. Polymer 1995, 36, 2407; (b) Mezghani, K.; Phillips, P. Polymer 1997, 38, 5725.
14. Piccarolo, S.; Sain, M.; Brucato, V.; Titomanlio, G. J Appl Polym Sci 1992, 46, 625.
15. Alamo, R. G.; Kim, M. H.; Galante, M. J.; Isasi, J. R.; Mandelkern, L. Macromolecules 1999, 32, 4050.
16. Auriemma, F.; De Rosa, C. Macromolecules 2002, 35, 9057.
17. Toman, R.; Wang, C.; Kressler, J.; Mülhaupt, R. Macromolecules 1996, 29, 8425.
18. Toman, R.; Semke, H.; Maier, R. D.; Thomann, Y.; Sherble, J.; Mülhaupt, R.; Kressler, J. Polymer 2001, 42, 4597.
19. Pérez, E.; Zucchi, D.; Sacchi, M. C.; Forlini, F.; Bello, A. Polymer 1999, 40, 675.
20. Alamo, R. G.; Blanco, J. A.; Agarwal, P. K.; Randall, J. C. Macromolecules 2003, 36, 1559.
21. Alamo, R. G.; Ghosal, A.; Chatterjee, J.; Thompson, K. L. Polymer 2005, 46, 8774.
22. De Rosa, C.; Auriemma, F.; Resconi, L. Macromolecules 2005, 38, 10080.
23. Mezghani, K.; Phillips, P. J. Polymer 1998, 39, 3735.
24. Supaphol, P. J Appl Polym Sci 2000, 78, 338.
25. Xu, W.; Liang, G.; Wang, W.; Tang, S.; He, P.; Pan, W. P. J Appl Polym Sci 2003, 88, 3093.
26. Wang, Y.; Liu, M.; Wang, Z.; Li, X.; Zhao, Q.; Fu, P. F. J Appl Polym Sci 2007, 104, 1415.
27. Yang, G. Z.; Chen, X.; Wang, W.; Wang, M.; Liu, T.; Li, C. Z. J Polym Sci Part B: Polym Phys 2007, 45, 976.
28. Wunderlich, B. Macromolecular Physics; Academic: New York, 1976; Vol. 2, p 115.
29. Ozawa, T. Polymer 1972, 12, 150.
30. Liu, T.; Mo, Z.; Wang, S.; Zhang, H. Polym Eng Sci 1997, 37, 569.
31. Kissinger, H. E. J Res Natl Bur Stand 1956, 57, 217.
32. Zhang, Y.; Xin, Z. J Appl Polym Sci 2006, 101, 3307.
33. Atanasov, A.; Nedkov, E. Commun Dept Chem 1984, 17, 143.
34. Nedkov, E.; Dobreva, T. e-Polymers 2003, 35, 1.
35. Grozdanov, A.; Buzarovska, A.; Bogoeva-Gaceva, G.; Nedkov, E. J Polym Sci Part B: Polym Phys 2005, 43, 66.
36. Hoffman, J. D.; Lauritzen, J. I.; Passaglia, E.; Ross, G. S.; Froten, F. J.; Weeks, J. J. Kolloid Z Z Polym 1969, 231, 564.
37. Clark, E. J.; Hoffman, J. D. Macromolecules 1984, 17, 878.
38. Wang, Y. F.; Lloyd, D. R. Polymer 1993, 34, 4740.
39. Cheng, S. Z. D.; Janimak, J. J.; Zhang, A.; Cheng, H. N. Macromolecules 1990, 23, 298.